A theoretical model for multi-layer jamming systems

Highlights

A theoretical model for multi-layer jamming systems

Fabio Caruso, Giacomo Mantriota, Luciano Afferrante, Giulio Reina

- A theoretical model to predict stiffness change in multi-layer jamming structure is presented
- The model captures the nonlinear behavior with a piecewise linear approximation
- Analytical predictions are in a good agreement with FEM simulations
- Force and deflection at full-slip increase with friction coefficient and vacuum pressure
- Deflection at full-slip is independent of the number of layers

A theoretical model for multi-layer jamming systems

Fabio Caruso, Giacomo Mantriota, Luciano Afferrante, Giulio Reina

[a]*Department of Mechanics, Mathematics and Management, Polytechnic University of Bari, Via E. Orabona 4, 70125, Bari, Italy,*

Abstract

On-demand stiffening methods are receiving increasing attention from the soft robotics community, due to the need of both flexibility and stiffness in many applications. Among the various methods, jamming-based techniques became very popular thanks to features such as fast and reversible transition between flexible and rigid states and easy fabrication. However, an analytical model of these structure, taking into account the nonlinearities involved in the change in stiffness, is a challenging task. In this effort, we propose an analytical model for predicting the change in the bending stiffness of a multi-layer jamming structure. We then compare our model with finite elements simulations, showing a very good agreement. The proposed model captures the intrinsic mechanics of these systems and provides a powerful tool for properly design their response to meet the requirement needed for a specific application.

Keywords: Multi-layer jamming, theoretical model, variable stiffness, controllable stiffness, wearable robotics, soft robotics, vacuum jamming

1. Introduction

Inspired by nature, in the past years, many researchers focused their attention on controlling mechanical properties on-demand [1]. This is particularly crucial in the field of soft robotics where both flexibility and stiffness are required in many applications [2][3][4], including minimally invasive surgery (MIS) [5], rehabilitation [6], exoskeletons [7], haptic interfaces [8], soft grippers [9], locomotion [10] and aerospace [11].
Stiffness modulation have been demonstrated using different strategies, for example thermal activation [12], electric[13] or magnetic field stimulation [14]. However, jamming-based methods are gaining increasing attention due

to their specific characteristics: fast and reversible transition between flexible and rigid states almost without a change in volume, cost-effectiveness, easy fabrication, easy to scale and lightweight [15][16][17][18]. Layer jamming typically consists of layers of compliant materials, such as sheets of paper or plastic (PET), placed in a airtight bag and connected to a vacuum regulator [19][20]. In these structures, the change in stiffness is governed by the slip at the interfaces between the layers [21][22][23]. The response of the structure to an external load can be divided in three major phases: a pre-slip phase, a partial-slip phase and a full-slip phase, as shown in Figure 1.

While this behavior has been studied and analytically modeled for a two-layer jamming structure [24], to the best of author's knowledge no studies presented an analytical model extended to the case of an arbitrary number of layers, which are the structures used in real-world applications. In this work, we propose a simple analytical 2D model based on a piecewise linear approximation to reproduce the response of a multi-layer jamming structure

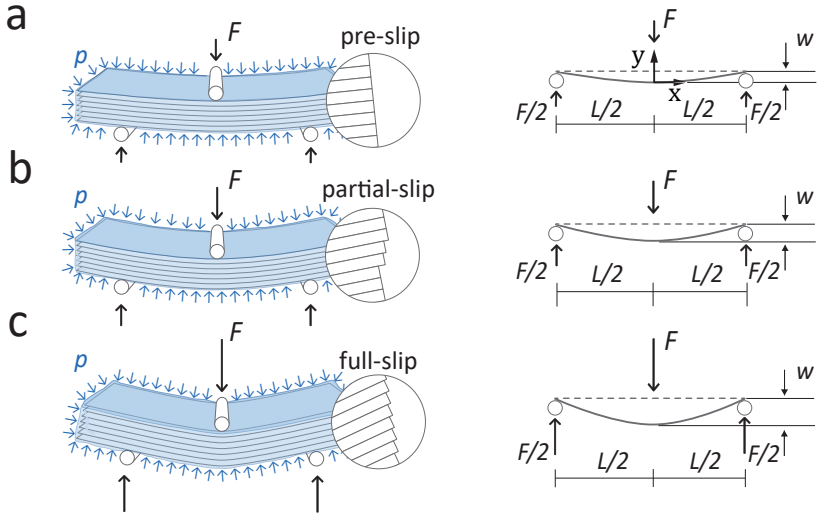

Figure 1: Schematic representation of the three deformation phases experienced by a multi-layer jamming structure.
a) Pre-slip phase, in which the bending stiffness is maximal and there is no-slip at the interfaces between the layers.
b) Partial-slip phase, in which some interfaces starts to slip, causing a progressive reduction in the bending stiffness.
c) Full-slip phase, in which all the layers are in slip causing the bending stiffness to be minimal.

when subjected to a 3-point bending test. The predictions of our analytical model were then compared with the results of 2-D finite element simulation, showing a good agreement. As the number of layers increases, the computational cost of the finite element simulations can be very expensive, thus an analytical model is extremely important because enables researchers to rapidly and accurately predict the response of these structures. Finally, we have analyzed the effect of the main design parameters (i.e., number of layers, vacuum pressure and coefficient of friction) on the bending stiffness of the structure in all the three deformation phases, which provide important information for mechanical optimization of materials, dimensions and operating conditions that are extremely useful in many applications, such as rehabilitation devices, exoskeletons and soft grippers [25].
The paper is organized as follows. We first present the derivation of the analytical model with all the assumptions in Section 2. In the same section we present the formulation of the finite element method used to validate the proposed model. Then in Section 3 our analytical predictions are compared with the results of finite element simulations. Finally Section 4 contains the conclusions.

2. Methods

2.1. Analytical modelling

Consider a layer-jamming structure with an arbitrary number of layers n, subjected to a 3-point bending test. Let the structure be subjected to a vacuum pressure p. As the load F increases, the structure experiences three different deformation phases Figure 1: a) A pre-slip phase, in which the longitudinal shear stress at the interfaces between layers remains below the static friction limit (μP). b) A partial-slip phase, in which the structure can be considered divided in two parts. An external cohesive region, where the longitudinal shear stress at the interfaces between two adjacent layers remains below the friction limit, and an internal slip region where the longitudinal shear stress at the interfaces equals the maximum admissible shear stress. As a result, layers in the internal region are in slip while those of the external region remains in stick regime. c) A full-slip phase, in which all the layers are in slip. Depending on the deformation phase, the stiffness of the structure will be different. To describe this behavior, we assume that the layers height is considerably smaller than its length and width, the structure undergoes small deflections, and the deformations are restricted to the xy

plane. Therefore, we model the layers using the Euler-Bernoulli beam theory, as this is a commonly adopted model for this problem [24][26] . Also, we neglect edge effects and interactions between layers and the membrane and we assume that the coefficient of friction μ and the pressure p are constant along the interfaces. Under this assumption, the relationship between the deflection at the center of the structure w and the applied load F is given by the well known formula

$$w = \frac{FL^3}{48EI} \tag{1}$$

where E is the Young's modulus of the layers, I is the second moment of area and L is the length of the structure. During the pre-slip and full-slip phases, the value of I is already known in literature and can be expressed by

$$I_{pre-slip} = \frac{b(nh)^3}{12} \tag{2}$$

$$I_{full-slip} = \frac{nbh^3}{12} \tag{3}$$

where b and h are the width and the height of a single layer and n is the total number of layers. However, to the best of author's knowledge, no studies investigated the computation of the bending stiffness during the partial-slip phase and the critical transverse loads at which slip occurs.

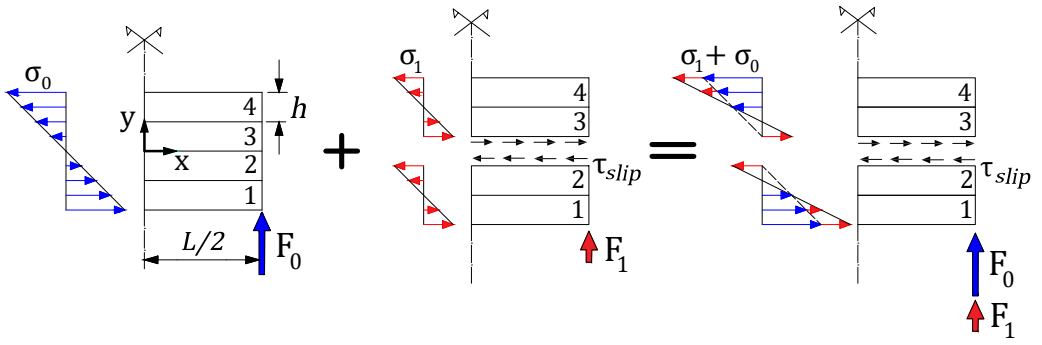

Figure 2: Schematic representation of the transverse loads, axial and longitudinal shear stresses in a four-layer jamming structure. F_0 is the transverse load at which layers 2 and 3 start to slip. F_1, instead, is the additional transverse force needed to cause slip between layers 1-2 and 3-4.

2.1.1. 4-Layer-jamming structure

First let us consider the four layer-jamming structure shown in Figure 2. Due to the load and geometry symmetry, we put our attention only on one half of the structure. As already mentioned, in the pre-slip phase, the whole structure behaves as a single beam. Therefore, the relationship between the resultant moment at each cross-section and the axial stress distribution is given by the Navier equation,

$$\sigma(x, y) = \frac{y\, M\,(x)}{I_{pre-slip}} \tag{4}$$

where *M(x) = F(L/2-x)/2* is the resultant moment and y is the distance from the neutral axis. As the load F increases the longitudinal shear stress at the interfaces will rise as a consequence. According to the Jourasky formula applied to rectangular cross-sections, the maximum shear stress occurs at the central interface and is given by

$$\tau_{slip} = \frac{3\, F_0}{2\, A} \tag{5}$$

where F_0 is the maximum load before slip occurs and $A = 4bh$ is the cross-section area. As the maximum possible shear stress at the interfaces is equal to the frictional limit (μp), the value of F_0 can be expressed as

$$F_0 = \frac{2\, \mu\, p\, A}{3} \tag{6}$$

The corresponding maximum value of the axial stress σ_0 occurs at $x = 0$, $y = 2h$,$F = 2F_0$, i.e.,

$$\sigma_0 = \sigma(0, 2h) = \frac{3F_0\, L}{16\, b\, h^2} \tag{7}$$

Equation (5) can be also expressed as a function of σ_0 indeed, from the static equilibrium of the upper half of the beam along the x-axis we obtain

$$\tau_{slip} = \mu p = \frac{2\sigma_0\, h}{L} \tag{8}$$

When the transverse load reaches the critical value F_0, the interface between layers 2 and 3 starts to slip. For successive load enhancements, we can assume that the structure is divided in two beams which experience the same deflection and are subjected to the same stress state. The axial stress

distribution, in this case, could be seen as the sum of the distribution in the pre-slip phase, caused by F_0, and the distribution generated by an additional force, (as shown in Figure 2). As the transverse load increases, the longitudinal shear stress between the interfaces that are still in full stick will grow. In order to find the value of the additional force F_1 that causes slip, we need to derive an expression for the longitudinal shear stress at the interfaces between layers 1-2 and 3-4 as a function of σ_0 and σ_1. Solving the static equilibrium of layers 1 and 4 along the longitudinal direction, we obtain

$$\tau_{1-2} = \tau_{3-4} = \frac{h}{L}\left(\sigma_0 + 2\sigma_1\right) \tag{9}$$

Equating (8) and (9) and solving for σ_1, we get $\sigma_1 = \sigma_0/2$ and hence in terms of the external transverse loads

$$F_1 = \frac{F_0}{4} \tag{10}$$

Table 1 and Figure 3 summarizes the relationships between the applied load F, the second moment of area I and the deflection at the center of the structure w, during the three deformation phases.

	Pre-slip	Partial-slip	Full-slip
F	$F < 2F_0$	$2F_0 < F < 2\left(F_1 + F_0\right)$	$F > 2\left(F_0 + F_1\right)$
I	$I_{pre-slip} = \frac{b\,(4h)^3}{12}$	$I_{partial-slip} = \frac{2b\,(2h)^3}{12}$	$I_{full-slip} = \frac{4b\,h^3}{12}$
w	$w = \frac{FL^3}{48EI_{pre-slip}}$	$w = \frac{(F-2F_0)L^3}{48EI_{partial-slip}}$	$w = \frac{(F-2(F_0+F_1))L^3}{48EI_{full-slip}}$

Table 1: Relationships between the applied load F, the second moment of area I and the deflection at the center of the structure w, during the three deformation phases of a four-layer jamming structure

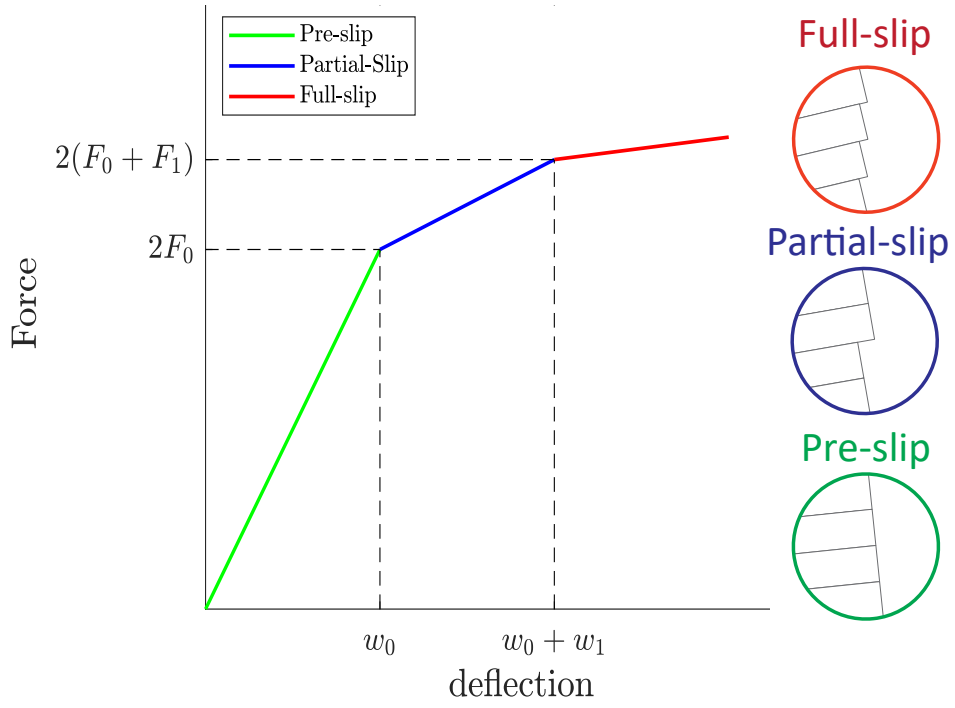

Figure 3: A conceptual representation of the force versus deflection relation for a four-layer jamming structure subjected to a three-point bending test

2.1.2. n-Layer-jamming structure

Consider a more general case, in which the number of layers n is an arbitrary even number. Due to the symmetry of the problem after the first slip, we can further simplify the formulation considering only the upper half of the structure. Compared to the previous case, there are multiple interfaces at which the slip could occur. In order to determine the first interface that reaches the frictional limit we need to calculate the longitudinal shear stress $\tau(0, y)$ at the cross section x=0 by solving the static equilibrium along the longitudinal direction for a generic portion of the structure of length $L/2$ and height H-y, which returns

$$\tau(0, y) = \frac{\sigma_0 + 2\sigma_1 y/H + \sigma_0 y/H}{L} H(1 - y/H) \tag{11}$$

where H is the height of upper half of the structure, L is the length of the entire structure and σ_0 and σ_1 are the axial stresses caused by the transverse

loads F_0 and F_1 (see Figure 4a). Now, equating (11) to the maximum value of the longitudinal shear stress ($\tau_{slip} = \sigma_0 H/L$) and solving for y/H, we obtain

$$\frac{\overline{y}}{H} = \frac{\frac{2\sigma_1}{\sigma_0}}{1 + \frac{2\sigma_1}{\sigma_0}} \tag{12}$$

where $\overline{y}$ is the height at which the shear stress of slip τ_{slip} is reached. Figure 4b, shows $\overline{y}$ is a monotonically increasing function of σ_1/σ_0, so demonstrating that, the first interface that enters in slip is the one nearest to the center of the structure.

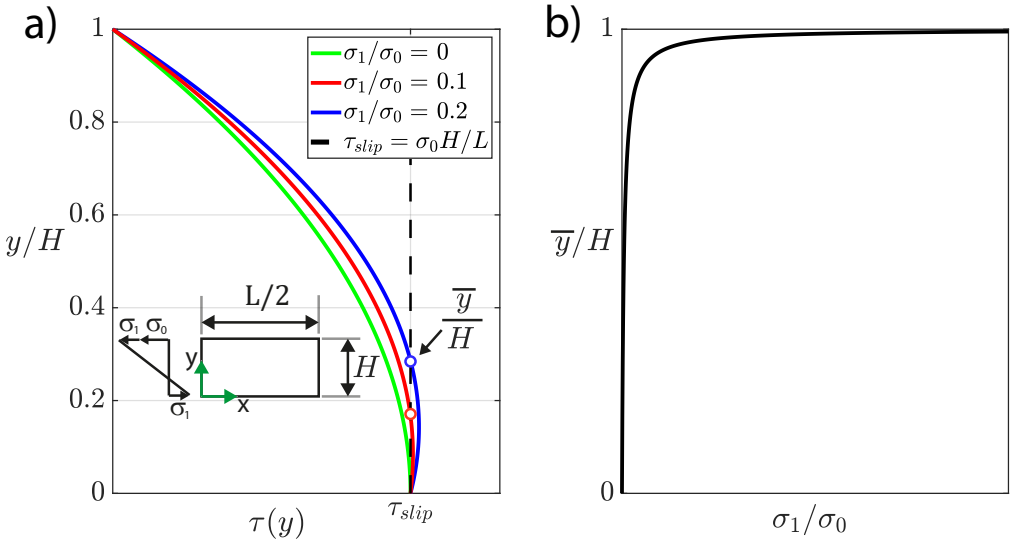

Figure 4: a) Longitudinal shear stress along the cross-section of the upper half of a multilayer jamming structure at $x = 0$, for three different values of σ_1/σ_0. b) Plot of equation (12)

Therefore, during the transition from pre-slip to full-slip, the structure can be described as divided in two parts. A cohesive region, in which the layers are attached to each other, and a slip region in which layers are detached, see Figure 5. Following the same procedure of the four-layer structure, we compute the value of the maximum axial stress σ_i and the corresponding additional transverse force F_i that causes slip at the i-th interface. Generalizing equation (9), we define an expression for $\tau(i)$, which is the longitudinal shear stress at the i-th interface

$$\tau(i) = \frac{\sigma_{top}(i) + \sigma_{int}(i)}{L}(H - ih) \tag{13}$$

where $\sigma_{int}(i)$ and $\sigma_{top}(i)$ are

$$\sigma_{int}(i) = \sigma_{bot}(i) + m(i)h \tag{14}$$

$$\sigma_{top}(i) = -\sigma_{top}(i-1) - \sigma_i \tag{15}$$

and $m(i)$ is given by

$$m(i) = \frac{\sigma_{top}(i) - \sigma_{bot}(i)}{H - (i-1)h} \tag{16}$$

Now, equating (13) to the maximum value of the longitudinal shear stress ($\tau_{slip} = \sigma_0 H/L$) and solving for σ_i, we obtain

$$\sigma_i = \frac{(H - h\,(i-1))\left(\frac{H\,\sigma_0}{2} + (H - h\,i)\left(\frac{\sigma_{int}(i-1)}{2} + \frac{\sigma_{top}(i-1)}{2} - \frac{h\,(\sigma_{int}(i-1) - \sigma_{top}(i-1))}{2\,(H - h\,(i-1))}\right)\right)}{h\,(H - h\,i)} \tag{17}$$

which is the value of the additional axial stress experienced by the layers in the cohesive region, which causes slip at the i-th interface. The expression of the corresponding additional transverse force F_i is given by

$$F_i = \frac{2\sigma_i\,(H - h\,(i-1))^2 + h^2\,\sigma_l(i)\;(i-1)}{6L} \qquad i = 1, ..., n/2 - 1 \tag{18}$$

where σ_l is the additional axial stress experienced by the layers that are already in slip.

$$\sigma_l(i) = \sigma_{int}(i) - \sigma_{int}(i-1) \tag{19}$$

The general expression of the second moment of area I during the partial-slip phase can be computed as follows

$$I_{partial-slip}(i) = 2\,\frac{b\,[(n/2 + 1 - i)\,h]^3}{12} + \frac{2\,b\,h^3}{12}(i-1) \qquad i = 1, ..., n/2 - 1 \tag{20}$$

where b and h are the width and height of a single layer and n is the total number of layers. Substituting (18) and (20) into (1) we obtain the additional deflection w_i caused by the additional force $2F_i$.

$$w_i = \frac{2F_i L^3}{48EI_{partial-slip}(i)} \qquad i = 1, ..., n/2 - 1 \tag{21}$$

Now, substituting (8) extended to the case of n layers ($\sigma_0 = \mu\, p\, L/(nh/2)$) into equation (17) and expressing the value of $\sigma_{top}, \sigma_{bot}, \sigma_{int}$ and σ_l as a function of $\mu\, p$, the formulas of the transverse forces and the corresponding deflections can be also expressed in terms of the coefficient of friction μ, vacuum pressure p, height h, width b, number of layers n, layers height h, Young modulus E and layers length L

$$F_0 = \frac{2\,\mu\, p\, b\, h\, n}{3} \tag{22}$$

$$F_1 = \frac{\mu\, p\, b\, h\, n}{3\,(n-2)} \tag{23}$$

$$F_2 = \frac{2\,\mu\, p\, b\, h\,(n^2 - 6\,n + 12)}{3\,(n^2 - 6\,n + 8)} \tag{24}$$

$$F_i = \frac{2\,\mu\, p\, b\, h\,(n^3 - 6\,(i-1)\,n^2 + 12\,(i-1)^2\,n - 8\,(i^3 - 3\,i^2 + 2\,i))}{3\,(n^3 - 6\,(i-1)\,n^2 + (12\,(i-1)^2 - 4)\,n - 8\,(i^3 - 3\,i^2 + 2\,i))} \qquad i = 3, ..., n/2{-}1 \tag{25}$$

$$w_0 = \frac{\mu\, p\, L^3}{3\,\mathrm{E}\, h^2\, n^2} \tag{26}$$

$$w_1 = \frac{2\,\mu\, p\, L^3}{3\,\mathrm{E}\, h^2\, n^2\,(n-2)} \tag{27}$$

$$w_2 = \frac{4\,\mu\, p\, L^3}{3\,\mathrm{E}\, h^2\, n\,(n^2 - 6\,n + 8)} \tag{28}$$

$$w_i = \frac{4\,\mu\, p\, L^3}{3\,E\, h^2(n^3 - 6\,(i-1)\,n^2 + (12\,(i-1)^2 - 4)\,n - 8\,(i^3 - 3\,i^2 + 2\,i))} \qquad i = 3, ..., n/2{-}1 \tag{29}$$

Table 2 summarizes the relationships between the applied load F, the second moment of area I, and the deflection at the center of the structure w, during the three deformation phases of a n-layer-jamming structure. Figure 5 show a schematic representation of the loads and stresses experienced by the structure in the partial-slip phase. In particular, in blue are indicated both the transverse load and the distribution of the axial stresses causing slip between layers i and *i-1*, while in red are indicated the additional transverse force and the distribution of the additional axial stresses producing slip between layers i and *i+1*.

	Pre-slip	Partial-slip	Full-slip
F	$F < 2F_0$	$2F_0 < F < 2\left(F_0 + \sum_{i=1}^{n/2-1} F_i\right)$	$F > 2\left(F_0 + \sum_{i=1}^{n/2-1} F_i\right)$
I	$I_{pre-slip} = \frac{b\,(nh)^3}{12}$	$I_{partial-slip}\,(i) = 2\,\frac{b\,[(n/2+1-i)\,h]^3}{12} + \frac{2\,b\,(i-1)\,h^3}{12}$	$I_{full-slip} = \frac{nb\,h^3}{12}$
w	$w = \frac{FL^3}{48EI_{pre-slip}}$	$w = \frac{F-2(\sum_{i=0}^{i-1} F_i)L^3}{48EI_{partial-slip}(i)}$	$w = \frac{(F-2(F_0+\sum_{i=1}^{n/2-1} F_i))L^3}{48EI_{full-slip}}$

Table 2: Relationships between the applied load F, the second moment of area I and the deflection at the center of the structure w, during the three deformation phases of a multi-layer jamming structure

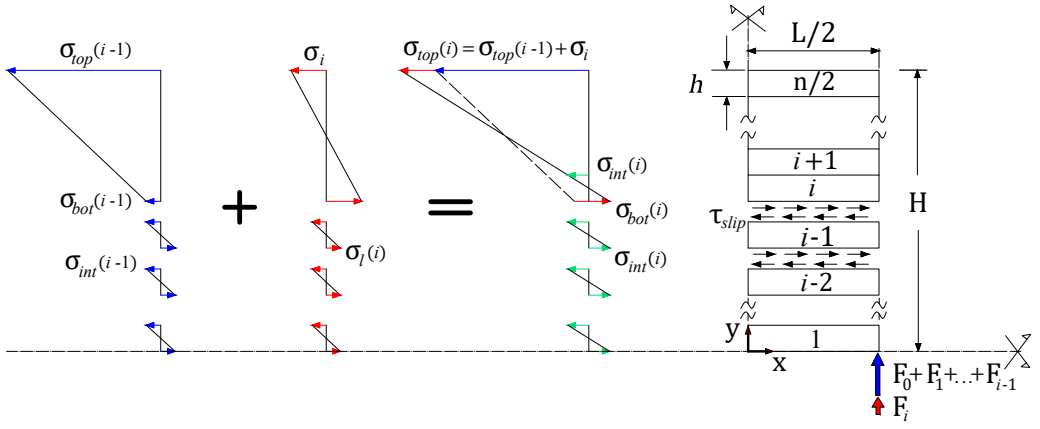

Figure 5: Schematic representation of the transverse loads, axial and longitudinal shear stresses in the partial-slip phase of a multi-layer jamming structure.

2.2. Finite Element formulation

To validate our analytical approach, a finite element model Figure 6 was developed. The simulations were performed using the commercial software ANSYS. Since all the loads and the corresponding deflections occur in the x-y plane, each layer was modeled with 2-D plane-strain elements (PLANE182). Each layer was meshed using a square four node plane strain element with a side length equals to half of the layer height, as done in the work of Narang et al. [24]. The interaction between two adjacent layers was modeled using the elements CONTA172 and TARGE169 with a constant coefficient of friction based on Coulomb's Law. The vacuum pressure was applied through a uniform distributed load acting on all the external surfaces of the structure. Due to the symmetry of the problem, the computational cost of the simulation was reduced considering only one half of the structure. For this reason, a zero horizontal displacement boundary condition was applied at the nodes on the center of the structure. Furthermore, vertical displacement was constrained at the end of the structure at the central interface. Finally, an incremental downward vertical displacement was applied at the first node of the top surface.

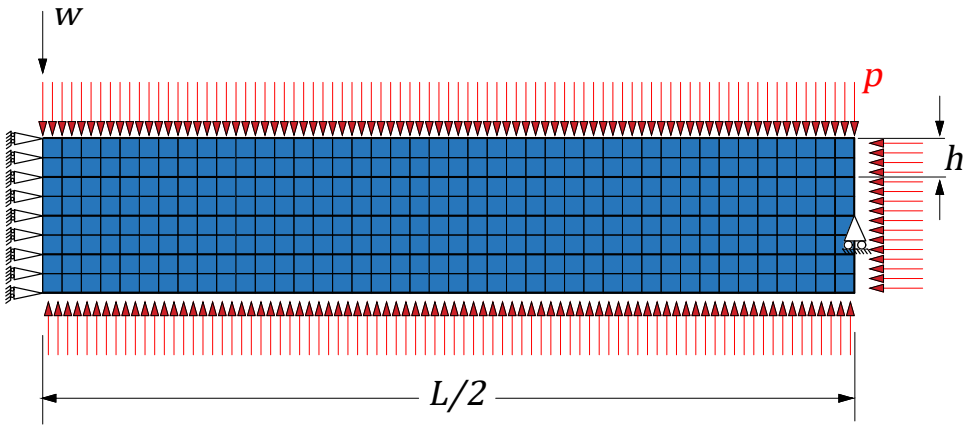

Figure 6: 2-D finite element model overview

3. Results

In this section, we present a comparison between the predictions of our analytical model and the results obtained by the 2-D FE analysis. In particular, we investigate the effect of the main design inputs (i.e., number of layers,

vacuum pressure and coefficient of friction) on the relationship between the applied load F and the deflection w at the center of the structure in a 3-point bending test.

3.1. Effect of the number of layers

In order to study the effect of the number of layers on the bending stiffness of the structure, we have carried out five simulations in which the number of layers n was varied from 4 to 20 in increments of four. In all simulations, geometric and material properties were chosen in accordance with the typical range of values used in layer-jamming applications [27], that are: height $h = 0.5\,[mm]$, length $L = 100\,[mm]$, width $b = 50\,[mm]$, Young's modulus $E = 6\,[GPa]$, Poisson's ratio $\nu = 0.156$. In addition, a vacuum pressure $p = 50\,[kPa]$ was applied on the external surfaces and the coefficient of friction was set to $\mu = 0.5$. Notice that in the analytical model the elastic modulus E was replaced by the plane-strain Young's modulus $\overline{E} = \frac{E}{1-\nu^2}$ as $b >> h$. As shown in Figure 7, the predictions of our analytical model are in good agreement with the results obtained by the finite element simulations. Notice that the red dots have coordinates (w_i,F_i) and represent the transition loads and the corresponding deflections at which change in bending stiffness occurs, due to slip at the i-th interface. As expected, in the pre-slip phase, the bending stiffness of the structure is proportional to n^3 as shown in (2). In addition, the force F_0 and the deflection w_0, at which the first slip occurs, are proportional to n and $1/n^2$ respectively. These dependencies are already known in literature and have been validated both with experiments and finite element simulations [24]. As the load F increases, the structure enters in the partial-slip phase and the force versus deflection relationship becomes non-linear. In our model we capture this behavior with a piece-wise linear approximation, in which the gradual change in stiffness and the transition loads at which this change occurs are described by equation (20) and (18), respectively. Thanks to this approach, we are also able to predict the last transition load at which the structure enters in the full-slip phase. Its expression is given by

$$F_{full-slip} = 2\,(F_0 + \sum_{i=1}^{n/2-1} F_i) \tag{30}$$

where F_0 and F_i are given by (6) and (18), respectively. As shown in Figure 7, the value of $F_{full-slip}$ scales with n. In addition, another interesting

results is that the deflection $w_{full-slip}$ at which the structure enter in the full-slip phase does not depend on the number of layers. The analytical expression of $w_{full-slip}$ is given by

$$w_{full-slip} = w_0 + \sum_{i=1}^{n/2-1} w_i \tag{31}$$

where w_0 is the deflection at which the structure shifts from the pre-slip to the partial-slip phase, while w_i, expressed in (21), is the additional deflection caused by the additional force F_i. With reference to Figure 7, the difference between the slope of the last segment (full-slip phase) and that of the previous one (last stage of the partial-slip phase) reduces as the number of layers increases. As a result, the percentage variation of the bending stiffness, which is proportional to the slope of the segments, becomes negligible when the number of layers is sufficiently large. Furthermore, most of the change in the bending stiffness is confined to a small range of deflections. Finally, we notice the percentage difference between the values of $F_{full-slip}$ given by our analytical model and the corresponding values obtained by FEM simulations slightly increases with the number of layers. One of the main reasons of such increase is probably due to the overall growth in the height of the structure. Indeed, the more the height increases the more we move away from the Euler-Bernoulli assumption $h << L$. In addition, a second source of error could be due to the stress concentration occurring near the supports and the applied load, which is observed to increase with the number of layers.

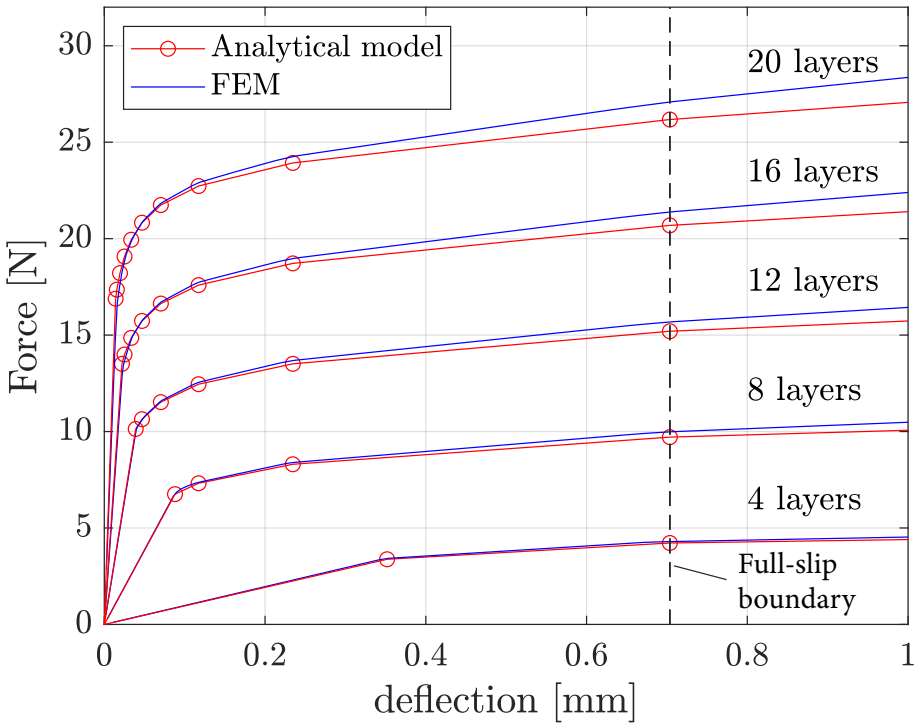

Figure 7: The force vs. deflection relation for a multi-layer jamming structure with different number of layers. Analytical predictions (red) are compared with FEM results (blue).

3.2. Effect of the vacuum pressure

To investigate the effect of the vacuum pressure on the bending stiffness of the structure, we have performed five simulations in which the vacuum pressure was varied from 20 to 100 [kPa] in increments of 20 [kPa]. The number of layers was kept constant and equals to $n = 20$ and all the other variables were maintained equal to the previous set of simulations. Figure 8 shows the comparison between the analytical and numerical results. As expected, the bending stiffness in the pre-slip phase does not depend on the vacuum pressure, as the structure is cohesive such phase. However, both the first transition force F_0 and the corresponding deflection w_0 scale with the vacuum pressure p. It is also interesting to notice that $F_{full-slip}$ and $w_{full-slip}$ are proportional to the vacuum pressure p.

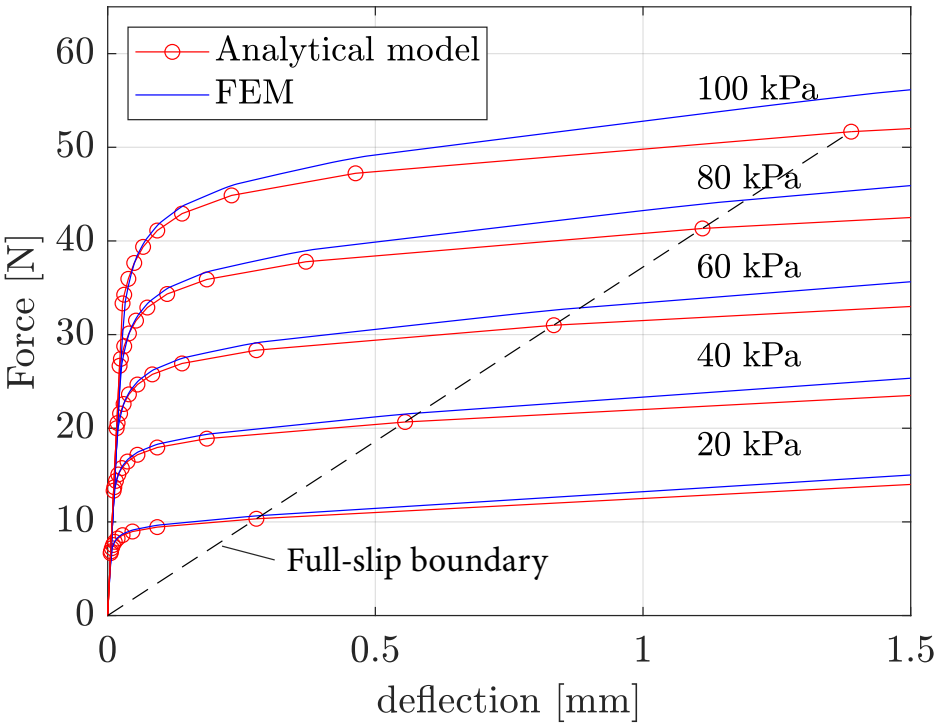

Figure 8: The force vs. deflection relation for a 20-layer jamming structure with different values of the vacuum pressure. Analytical predictions (red) are compared with FEM results (blue).

3.3. Effect of the coefficient of friction

To investigate the effect of coefficient of friction on the bending stiffness of the structure, we have performed five simulations in which the coefficient of friction μ was varied from 0.2 to 0.6 in increments of 0.1. The number of layers and the vacuum pressure were kept constant and equals to $n = 20$ and $p = 50\,[kPa]$, respectively. All the other variables were maintained equal to the first set of simulations. Figure 9 shows the comparison between the analytical and numerical results. As expected, changing either the coefficient of friction or the vacuum pressure produces the same effect on the general behavior of the structure. Similar to the previous case, the slope of the curve (which is proportional to the bending stiffness) in the pre-slip phase does not depend on the coefficient of friction because no interface is sliding. On the contrary the forces of first slip F_0 and full slip $F_{full-slip}$ (and corresponding

deflections) linearly increase with μ.

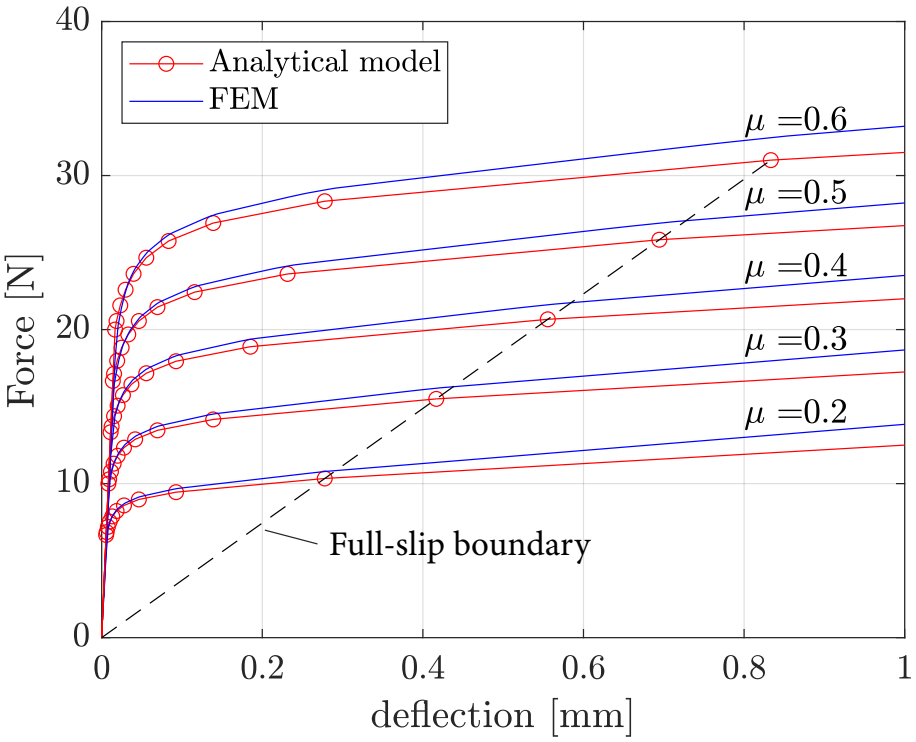

Figure 9: The force vs. deflection relation for a 20-layer jamming structure with different values of the coefficient of friction. Analytical predictions (red) are compared with the FEM results (blue).

Finally, Figure 10 shows FEM results of the three deformation phases experienced by an 8-layer structure. While in the pre-slip stage (Figure 10(a)) all layers are still attached, in the partial-slip phase (Figure 10(b)) two different regions can be observed: an inner region, in which layers are in slip, and an outer region where the layers are still in stick regime. These results confirmed our hypothesis that slip propagates from the inner to the outer interfaces. Finally, the full-slip phase in which all the layers are in slip is shown in Figure 10(c). For the sake of readability, only the right-end portion of the structure is shown.

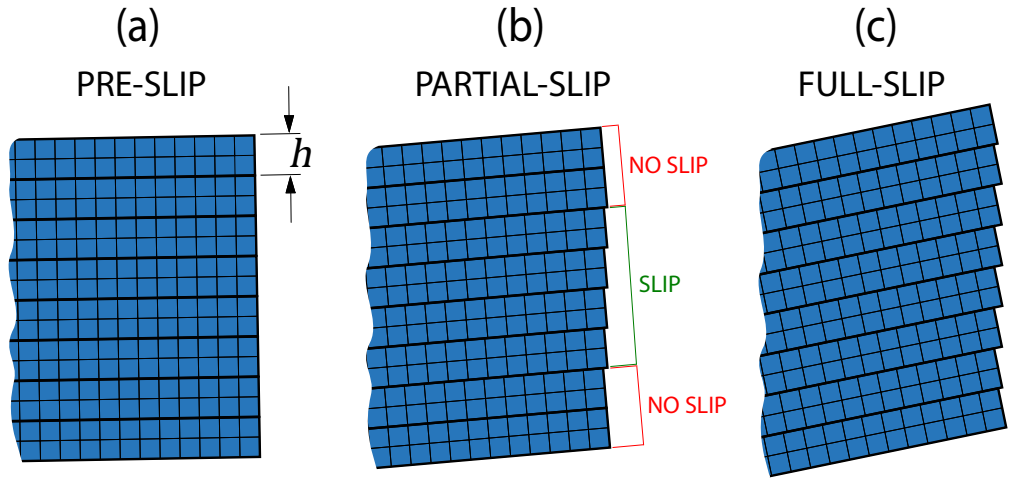

Figure 10: Deformation phases in a 8-layer structure extracted from FEM simulations: a) pre-slip phase in which all the layers are attached, b) partial-slip phase in which the layers in the inner region are in slip (green bracket) while the layers in the outer region are still attached (red brackets) c) full-slip phase in which all the layers have slipped.

4. Conclusion

In this work, we presented a 2D analytical model for predicting the change in the bending stiffness of a multi-layer jamming structure when subjected to a 3-point bending test. Previous works introduced analytical models limited to the case of two-layers jamming structures and extended the analysis to multi-layer structures using only finite elements models.
In contrast, our analytical model predicted the change in stiffness as well as the transition loads and the corresponding deflections of a structure with an arbitrary number of layers. In particular, the model is able to capture the nonlinear change in stiffness in the partial-slip phase, with a piecewise linear approximation that represents one of the main contributions of this work.
Furthermore we have demonstrated that slip starts at the central interface and propagates form the center to the end of the structure, forming two separate regions: an inner region, in which layers are in slip and an outer region where layers are still attached.
In order to keep the complexity of the model at an acceptable level, we used the Euler-Bernoulli beam theory to model the layers and computed all the equilibria in the undeformed configuration. We validated our model comparing it with 2D finite element simulations, showing a good agreement for small

deflections.
Our formulation is simple and computationally efficient compared to the finite element model, in which the computational time increases with the number of layers and the solution could take hours to converge.
We have finally investigated the effect of the main design inputs (i.e, number of layers, coefficient of friction and vacuum pressure) on the bending stiffness of the structure. We have found that the deflection at which the structure enters in the full-slip phase is independent of the number of layers and that force and deflection at full-slip increase with the friction coefficient and vacuum pressure. The proposed model is computationally cheap and can accurately capture the intrinsic mechanics of these systems, providing a powerful tool for properly design their response to meet the requirement needed for a specific application.

References

[1] B. Vanderborght, A. Albu-Schäffer, A. Bicchi, E. Burdet, D. G. Caldwell, R. Carloni, M. Catalano, O. Eiberger, W. Friedl, G. Ganesh, et al., Variable impedance actuators: A review, Robotics and autonomous systems 61 (12) (2013) 1601–1614.

[2] M. Manti, V. Cacucciolo, M. Cianchetti, Stiffening in soft robotics: A review of the state of the art, IEEE Robotics & Automation Magazine 23 (3) (2016) 93–106.

[3] L. Wang, Y. Yang, Y. Chen, C. Majidi, F. Iida, E. Askounis, Q. Pei, Controllable and reversible tuning of material rigidity for robot applications, Materials Today 21 (5) (2018) 563–576.

[4] M. Cianchetti, T. Ranzani, G. Gerboni, T. Nanayakkara, K. Althoefer, P. Dasgupta, A. Menciassi, Soft robotics technologies to address shortcomings in today's minimally invasive surgery: the stiff-flop approach, Soft robotics 1 (2) (2014) 122–131.

[5] Y.-J. Kim, S. Cheng, S. Kim, K. Iagnemma, A novel layer jamming mechanism with tunable stiffness capability for minimally invasive surgery, IEEE Transactions on Robotics 29 (4) (2013) 1031–1042.

[6] Y. S. Narang, B. Aktaş, S. Ornellas, J. J. Vlassak, R. D. Howe, Lightweight highly tunable jamming-based composites, Soft robotics 7 (6) (2020) 724–735.

[7] Y. Shao, W. Zhang, Y. Su, X. Ding, Design and optimisation of load-adaptive actuator with variable stiffness for compact ankle exoskeleton, Mechanism and Machine Theory 161 (2021) 104323.

[8] Y. Park, I. Jo, J. Lee, J. Bae, Wehaptic: A wearable haptic interface for accurate position tracking and interactive force control, Mechanism and Machine Theory 153 (2020) 104005.

[9] E. Brown, N. Rodenberg, J. Amend, A. Mozeika, E. Steltz, M. R. Zakin, H. Lipson, H. M. Jaeger, Universal robotic gripper based on the jamming of granular material, Proceedings of the National Academy of Sciences 107 (44) (2010) 18809–18814.

[10] E. Steltz, A. Mozeika, J. Rembisz, N. Corson, H. Jaeger, Jamming as an enabling technology for soft robotics, in: Electroactive Polymer Actuators and Devices (EAPAD) 2010, Vol. 7642, International Society for Optics and Photonics, 2010, p. 764225.

[11] I. K. Kuder, A. F. Arrieta, W. E. Raither, P. Ermanni, Variable stiffness material and structural concepts for morphing applications, Progress in Aerospace Sciences 63 (2013) 33–55.

[12] J. Shintake, B. Schubert, S. Rosset, H. Shea, D. Floreano, Variable stiffness actuator for soft robotics using dielectric elastomer and low-melting-point alloy, in: 2015 IEEE/RSJ International Conference on Intelligent Robots and Systems (IROS), IEEE, 2015, pp. 1097–1102.

[13] F. Carpi, G. Frediani, C. Gerboni, J. Gemignani, D. De Rossi, Enabling variable-stiffness hand rehabilitation orthoses with dielectric elastomer transducers, Medical engineering & physics 36 (2) (2014) 205–211.

[14] C. Majidi, R. J. Wood, Tunable elastic stiffness with microconfined magnetorheological domains at low magnetic field, Applied Physics Letters 97 (16) (2010) 164104.

[15] B. Aktaş, Y. S. Narang, N. Vasios, K. Bertoldi, R. D. Howe, A modeling framework for jamming structures, Advanced Functional Materials 31 (16) (2021) 2007554.

[16] D. S. Shah, E. J. Yang, M. C. Yuen, E. C. Huang, R. Kramer-Bottiglio, Jamming skins that control system rigidity from the surface, Advanced Functional Materials 31 (1) (2021) 2006915.

[17] M. Brancadoro, M. Manti, S. Tognarelli, M. Cianchetti, Fiber jamming transition as a stiffening mechanism for soft robotics, Soft robotics 7 (6) (2020) 663–674.

[18] T. Hou, X. Yang, Y. Aiyama, K. Liu, Z. Wang, T. Wang, J. Liang, Y. Fan, Design and experiment of a universal two-fingered hand with soft fingertips based on jamming effect, Mechanism and Machine Theory 133 (2019) 706–719.

[19] M. Ibrahimi, L. Paternò, L. Ricotti, A. Menciassi, A layer jamming actuator for tunable stiffness and shape-changing devices, Soft Robotics 8 (1) (2021) 85–96.

[20] X. Zeng, C. Hurd, H.-J. Su, S. Song, J. Wang, A parallel-guided compliant mechanism with variable stiffness based on layer jamming, Mechanism and Machine Theory 148 (2020) 103791.

[21] Y. S. Narang, A. Degirmenci, J. J. Vlassak, R. D. Howe, Transforming the dynamic response of robotic structures and systems through laminar jamming, IEEE Robotics and Automation Letters 3 (2) (2017) 688–695.

[22] I. Choi, N. Corson, L. Peiros, E. W. Hawkes, S. Keller, S. Follmer, A soft, controllable, high force density linear brake utilizing layer jamming, IEEE Robotics and Automation Letters 3 (1) (2017) 450–457.

[23] W. H. Choi, S. Kim, D. Lee, D. Shin, Soft, multi-dof, variable stiffness mechanism using layer jamming for wearable robots, IEEE Robotics and Automation Letters 4 (3) (2019) 2539–2546.

[24] Y. S. Narang, J. J. Vlassak, R. D. Howe, Mechanically versatile soft machines through laminar jamming, Advanced Functional Materials 28 (17) (2018) 1707136.

[25] J. Shintake, V. Cacucciolo, D. Floreano, H. Shea, Soft robotic grippers, Advanced Materials 30 (29) (2018) 1707035.

[26] R. Acevedo, L. Santos, R. Pedersen, N. Goyal, N. Bruck, S. Gupta, H. Bruck, Characterization and modeling of layer jamming for designing engineering materials with programmable elastic-plastic behavior, Experimental Mechanics 60 (9) (2020) 1187–1203.

[27] S. G. Fitzgerald, G. W. Delaney, D. Howard, A review of jamming actuation in soft robotics, in: Actuators, Vol. 9, Multidisciplinary Digital Publishing Institute, 2020, p. 104.